Lab on a Chip

PAPER

View Article Online
View Journal | View Issue

Cite this: *Lab Chip*, 2025, **25**, 2757

Development of a high-performance sliding microneedle-lateral flow immunoassay strip device for ultra-rapid point-of-care diagnosis†

Soo-bin Yu and Jae Hwan Jung *

Received 27th February 2025,
Accepted 13th April 2025

DOI: 10.1039/d5lc00199d

rsc.li/loc

Interstitial fluid (ISF) is a promising biofluid for non-invasive diagnostics, but its clinical application is limited by slow extraction rates and small sample volumes. To address these challenges, we developed the high-performance sliding microneedle-lateral flow immunoassay (HP-SML) device, an improved microneedle (MN)-based platform for rapid ISF extraction and on-site biomarker detection. The device incorporates extended MNs (1400 μm), a 3D-printed insertion case, and a lateral flow assay (LFA), enabling efficient ISF collection and immediate visual confirmation of test results. The HP-SML device demonstrated a 5-fold increase in ISF extraction speed compared to conventional SML devices, achieving 1.5 μL min^{-1} extraction rates with minimal tissue disruption and rapid skin recovery within 15 minutes. The device successfully detected C-reactive protein (CRP) at a clinically relevant limit of 10^4 ng mL^{-1}, confirming its applicability for Hodgkin lymphoma (HL) prognosis monitoring. It also exhibited high specificity for CRP, with no cross-reactivity observed against other inflammatory biomarkers such as IL-6, TNF-α, MMP-9, and MMP-2. Furthermore, ISF-derived CRP levels strongly correlated with serum CRP concentrations, validating ISF as a viable alternative for HL management. Given its high efficiency, ease of use, and on-site detection capabilities, the HP-SML device presents a significant advancement in point-of-care diagnostics and continuous disease monitoring.

1. Introduction

Interstitial fluid (ISF) is a colorless, water-like liquid that exists in the space between cells and blood vessels.[1] ISF contains many biomarkers found in plasma, as well as unique biomarkers absent in plasma, making it valuable for disease diagnosis.[2,3] Unlike blood, ISF can be collected with minimal discomfort as it is less invasive and does not clot, allowing for diagnostic testing without the need for preprocessing.[4,5] However, the volume of ISF that can be extracted is significantly smaller than that of blood, saliva, or urine,[6–8] necessitating the development of technologies capable of analyzing small amounts of ISF efficiently. Therefore, there is a critical need for a device that can efficiently extract ISF and rapidly detect biomarkers to facilitate diagnostic applications.

In a previous study, we developed the sliding microneedle (MN)-lateral flow immunoassay (LFA) integrated device (SML device) for ISF extraction with high sensitivity for biomarker detection.[9] However, limitations such as slow *in vivo* extraction speed, sample loss, contamination during device separation, and user inconvenience have been identified. To address these challenges, this study presents a user-friendly device that improves ISF extraction speed and biomarker detection efficiency, enhancing its potential for clinical applications. Specifically, we designed an MN-based device with an extended MN length (approximately twofold), enabling rapid ISF extraction while maintaining a stable vertical penetration depth. To validate its effectiveness, we targeted C-reactive protein (CRP), a biomarker for monitoring Hodgkin lymphoma (HL) relapse, and evaluated the device's performance.

HL is a lymphoid malignancy that primarily affects adolescents and young adults, accounting for approximately 10% of all lymphomas.[10–12] Most HL patients can be successfully treated with chemotherapy, but 10–30% experience relapse, necessitating ongoing monitoring and management to detect and address recurrence, even after an initial remission.[13–15] Positron emission tomography–computed tomography (PET/CT) is commonly used for the management and staging of HL; however, it is expensive, time-consuming, and not practical for continuous monitoring.[16,17] Therefore, there is a need for a technology that enables continuous, on-site management of HL in an inexpensive and convenient manner, such as point-of-care (POC) testing.[18]

CRP has been studied as an independent prognostic factor in the management of HL.[19–21] CRP is a nonspecific inflammatory marker,[22,23] which increases within 4–10 hours

Department of Pharmaceutical Engineering, Dankook University, Cheonan, Republic of Korea. E-mail: jjaehwan@dankook.ac.kr

† Electronic supplementary information (ESI) available. See DOI: https://doi.org/10.1039/d5lc00199d

after the onset of an inflammatory process and reaches a peak around 48 hours, with levels potentially increasing up to 1000 times higher than the baseline during acute inflammatory events.[24,25] CRP then declines with a half-life of approximately 19 hours.[24] These dynamic changes in CRP levels reflect the underlying inflammatory processes, making CRP a useful marker for disease management and monitoring in HL. Negreiros *et al.* reported that the 36 month progression-free survival (PFS) of HL patients with CRP levels less than 10^4 ng mL^{-1} after 6 cycles of chemotherapy was 91.7%, indicating that CRP concentrations can influence the prognostic management of HL.[26] Furthermore, studies by Wieland *et al.* and Li *et al.* confirmed that CRP concentrations hold prognostic value in the management of HL patients.[27,28] Typically, biomarkers such as CRP are analyzed using blood samples. However, blood collection requires trained medical professionals and complex equipment for sample processing, which limits its suitability for POC testing.[29]

To address these challenges, we developed the high-performance sliding microneedle-lateral flow immunoassay strip device (HP-SML Device), which integrates a metal MN-based ISF extraction system with a LFA biomarker detection system. Metal MNs offer greater mechanical strength than conventional MNs, enabling stable skin insertion with minimal force and reduced risk of breakage or deformation.[30–32] Meanwhile, LFA technology is a rapid, low-cost method for biomarker detection, making it ideal for POC testing applications.[33–35] Thus, we designed the HP-SML device to enable the POC HL monitoring by rapidly and conveniently detecting CRP in ISF. To achieve efficient ISF extraction, the MN was inserted at an angle, increasing the effective skin insertion area and enhancing extraction speed. Additionally, the vertical penetration depth was carefully controlled, preventing contamination from blood. To ensure consistent skin insertion angles, the MN was integrated into a 3D-printed device (Fig. 1A). Furthermore, to enable rapid and accurate CRP detection, the sample pad of the LFA was directly connected to the MN, ensuring that the absorbed ISF flowed seamlessly into the LFA without loss or contamination. The CRP detection results could be visually confirmed without disassembling the device, as the control and test lines on the LFAs were exposed (Fig. 1B). The detection limit for CRP was set at 10^4 ng mL^{-1}, based on a previous study.[26]

In this study, we demonstrate the development of a HP-SML device that significantly enhances ISF extraction speed through an extended metal MN design, while enabling rapid and cost-effective CRP detection. These advancements establish the HP-SML device as a promising solution for economic, ultra-rapid, and reliable POC HL relapse monitoring.

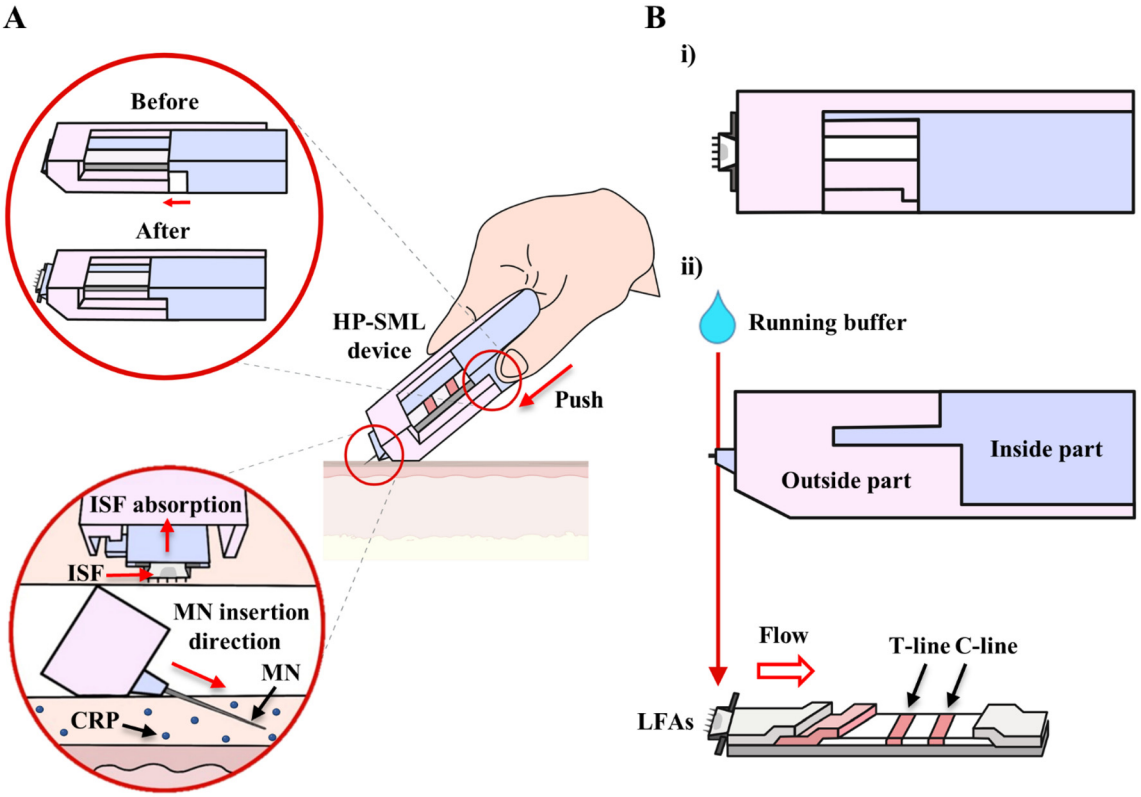

Fig. 1 Schematic illustrating the operation of the HP-SML device: (A) The MN penetrates the skin at a 34° angle when the Inside part on the left side is pushed with the thumb, extracting the skin ISF. (B) The extracted biomarkers in the ISF (i) are transferred to the LFAs by a running buffer and then detected (ii). All the schematics were created using BioRender.

2. Experimental

2.1. Materials

Stainless-steel MN arrays consisting of 1 × 5 MNs, each with a 1400 μm length and 200 μm base, were customized and purchased by SKB Tech (Fig. 2A). The filter paper was obtained from CHMLAB Group. Lateral flow strips for CRP detection, recombinant CRP antigen, and running buffer were purchased from Boreda Biotech Co., Ltd. Crystal violet (100 g) and sulforhodamine B (SRB) were bought from Sigma-Aldrich. The Sylgard 184 silicone elastomer curing kit (450 g/45 g) was obtained from DOW. Porcine skin (3 × 3 cm) was purchased from Cronex. The 50× TAE buffer and EB agarose were bought from LPS Solution. The sterile normal saline solution (1000 mL) was obtained from JW Pharmaceutical. Low-viscosity λ-carrageenan (1 g) was purchased from TCI. Sprague–Dawley (SD) rats (6 weeks, male, and 150–200 g) were bought from Samtako Bio Korea Co., Ltd.

2.2. Microneedle design

We hypothesized that increasing the MN length would enhance the surface area in contact with tissue, thereby leading to a faster and more stable ISF extraction rate. To test this hypothesis, the MN length was set to 1400 μm, approximately twice the length of the commonly used 750 μm MN,[36–39] and the base width was designed to be 200 μm.

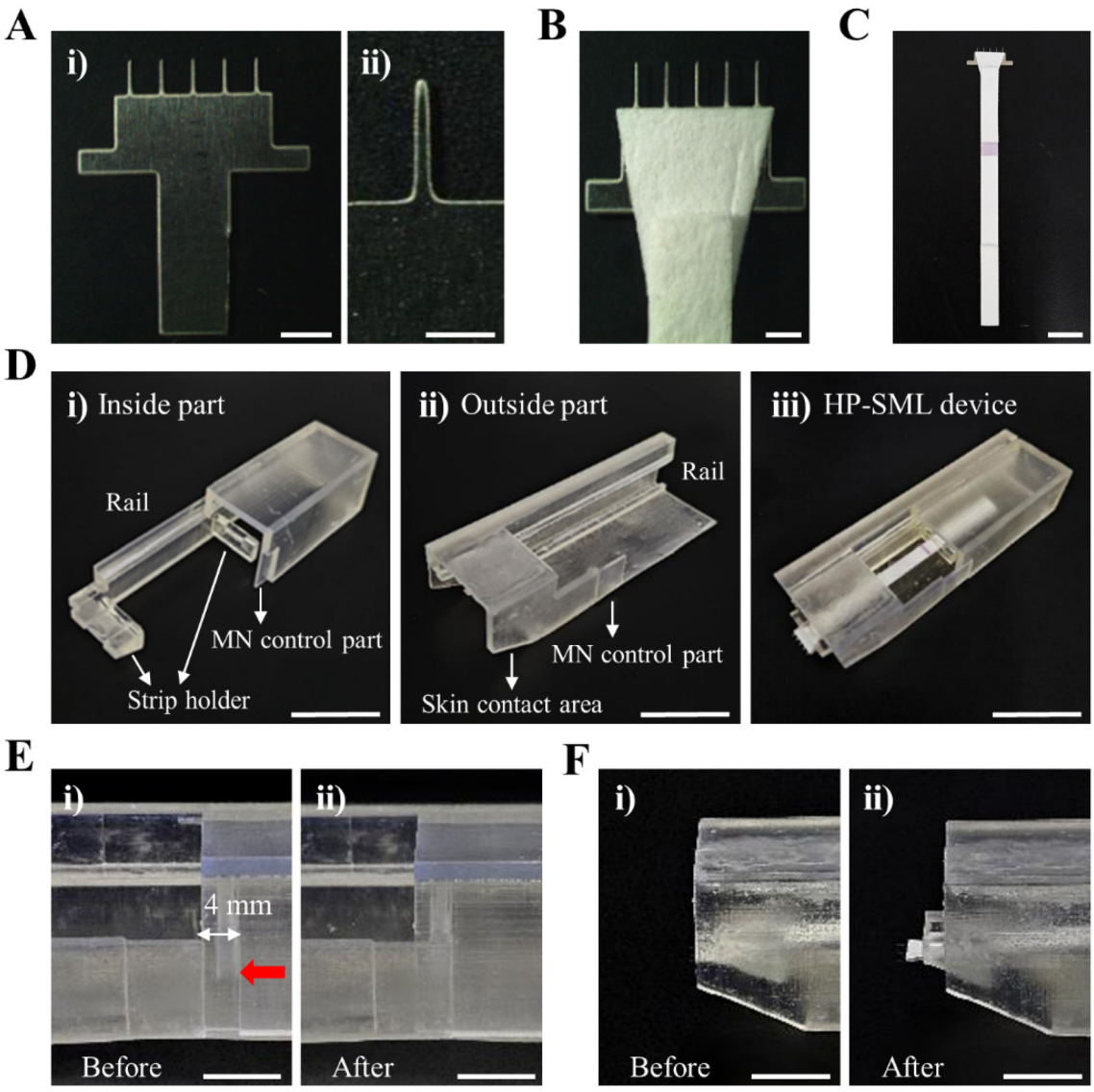

Fig. 2 (A) An optical image of a 1400 μm MN array (i) (scale bar = 2 mm) and a magnified image of a single MN (ii) (scale bar = 1 mm). (B) An optical image of the MN array attached to a filter paper reservoir (scale bar = 1 mm). (C) An optical image of the MN-LFAs (scale bar = 1 cm). (D) Optical images of the 3D printed cases of the HP-SML device: Inside part (i), Outside part (ii), and the assembled HP-SML device (iii) (scale bars = 2 cm). (E) Optical images of the MN control part before (i) and after (ii) pushing the Inside part for MN penetration to the skin (scale bars = 1 cm). (F) Optical images of the strip holder before (i) and after (ii) pushing the Inside part (scale bars = 1 cm).

At this extended MN length, the vertical penetration depth of the MN into the skin, when using the HP-SML device, was maintained at 750 μm. Consequently, the theoretical penetration angle (A) of the MN within the HP-SML device was calculated to be approximately 33°, based on the following equation (formula 1) (see Fig. S1†).

$$\sin A = \frac{B}{1400\ \mu\text{m}} \quad (1)$$

where A represents the insertion angle when a 1400 μm-long MN is inserted into the HP-SML device, and B represents the vertical penetration depth of the MN.

2.3. Fabrication of the HP-SML device

To rapidly deliver the ISF extracted through the MN to the strip, a trapezoidal filter paper (upper side 7 mm; lower side 3 mm; height 7 mm) was attached to the surface of the MN (Fig. 2B) and then positioned between the sample pads of the LFAs (Fig. 2C). To ensure accurate penetration angles and reproducibility during skin penetration with the MN, the case of the H-MNID-LI was designed using CAD (computer-aided design) software (3DS Max 2023) and printed using a stereolithography (SLA) 3D printer (Form 3, Formlabs, USA) (Fig. 2D). The device has overall dimensions of 77 × 24 × 19 mm and is shaped like a rectangular parallelepiped. It is primarily divided into two sections: the Inside part and the Outside part. The dimensions of the Inside part are 76 × 19 × 18 mm, and the dimensions of the Outside part are 77 × 24 × 19 mm. Two strip holders are incorporated into the Inside part to prevent the LFA strip from falling out when the MN is inserted (Fig. 2D(i)). Each strip holder consists of a small rectangular perforation within a larger rectangle, designed so that the strip fits securely into the hole. The perforation has dimensions of 6 × 2 × 2 mm to ensure the strip does not fall out, and the distance between the two fixing brackets is 14 mm.

Additionally, a 'skin contact area' is designed on the front lower surface of the Outside part to allow the device to be fixed flat against the skin (Fig. 2D(ii)). At this point, the MN insertion angle is fixed at 34°. Rails are incorporated on both the Inside and Outside parts to ensure precise alignment and combination of the two sections (Fig. 2D(iii)). The assembled HP-SML device was designed to penetrate the skin at a 34° angle by pushing the Inside part on the left side with the thumb (Fig. 2E). To ensure stable MN insertion, a 4 mm gap was maintained between the MN control parts of the Inside and the Outside parts, allowing the Inside part to move up to 4 mm (Fig. 2F).

2.4. Penetration stability test of the HP-SML device

A skin permeation reproducibility experiment of the HP-SML device was conducted using polydimethylsiloxane (PDMS) as a model for artificial skin.[40] PDMS was prepared by mixing a Sylgard 184 base and a curing agent in a 10 : 1 ratio by weight. The mixture was then degassed to remove air bubbles and cured in an oven at 85 °C for 2 hours. After curing, 40 μL of crystal violet solution was applied to the area where the MN was inserted into the PDMS using the HP-SML device for 10 minutes. The solution was then removed using an alcohol pad. The location of MN insertion was excised to examine the insertion angle and depth at the cross-section (n = 3). The observations and measurements were performed using a stereomicroscope (SZ61, OLYMPUS, and Japan) and analyzed with eXcope software (DIXI Optics, South Korea).

2.5. *Ex vivo* skin penetration test

To evaluate the skin penetration ability of the HP-SML device, the MN was inserted into porcine skin *ex vivo* for 5 seconds and then removed. Subsequently, the skin was stained with 20 μL of crystal violet solution for 10 minutes and then wiped clean with an alcohol pad. The skin penetration sites were observed using a stereomicroscope and analyzed with eXcope software (n = 3).

2.6. Quantification of ISF extraction using the HP-SML device

The ISF extracted through the HP-SML device is absorbed onto the filter paper on the MN, and the wetted area of the absorbed solution is correlated with the volume of the extracted ISF. Therefore, this experiment was conducted to quantify the volume of the extracted ISF based on the area occupied by the solution absorbed on the filter paper. First, a SRB solution was applied to the filter paper attached to the MN using a micropipette, with volumes ranging from 0 to 5 μL at intervals of 0.5 μL (n = 3). Images of the wetted areas of the solution were captured using a stereomicroscope and eXcope software, and the wetted area of the SRB solution was quantified using ImageJ software.

2.7. *In vitro* ISF extraction test

To confirm the ISF extraction ability of the HP-SML device, the wetted area of the filter paper was examined after applying it to a 1% (w/v) agarose gel for a specified time.[41] To determine the ISF extraction time as a function of MN length, the HP-SML device with needle lengths of 750 μm and 1400 μm were used, and the application time ranged from 0 to 80 seconds for the 750 μm HP-SML device and from 0 to 60 seconds for the 1400 μm HP-SML device, with observations of changes in the wetted area of the filter paper made at 10 second intervals (n = 3). The 1% (w/v) agarose gel was prepared by mixing 1 g of agarose with 100 mL of 0.5× TAE buffer containing 3.75 mg of SRB, heating until dissolved, and allowing the gel to solidify in a Petri dish for 1 hour before covering it with parafilm.[42] The wetted area of the filter paper was analyzed using ImageJ software.

2.8. Sensitivity test

To verify the sensitivity of the HP-SML device, a recombinant CRP antigen was prepared at concentrations of 0, 10, 10^2, 10^3, 10^4 and 10^5 ng mL^{-1}, respectively. According to the manufacturer's protocol for LFAs, the total volume for the

detection limit experiment was 100 μL, which included the CRP solution and running buffer. First, the detection limit experiment was performed on "single LFAs" where the MNs were not connected. A volume of 0.1 μL of CRP solution was added to the sample pad, followed by 99.9 μL of running buffer at the same location. The results were observed after 10 minutes (n = 10). The CRP solution volume was set to 0.1 μL to achieve the detection limit of 10^4 ng mL^{-1}, relevant for the prognosis management of HL patients.

Second, the detection limit was measured using "passive sample loading onto the HP-SML device." This experiment was conducted to determine whether the detection limit was affected by the integration of MNs with LFAs. A 0.1 μL aliquot of CRP solution was added to the filter paper of the HP-SML device using a micropipette, followed by the addition of 99.9 μL of running buffer. The detection results were recorded after 10 minutes (n = 10).

Third, the detection limit experiment was conducted using the HP-SML device on a 1% (w/v) agarose gel containing CRP. The HP-SML device was applied to agarose gels with CRP concentrations ranging from 0 to 10^5 ng mL^{-1} for 4 seconds to extract 0.1 μL of the solution. After application, 99.9 μL of running buffer was added to the filter paper, and the detection results were assessed after 10 minutes (n = 10). All detection limit experiments were analyzed by converting the test line of the strip to grayscale and quantifying the color intensity using ImageJ software.

2.9. Specificity test

To test the specificity of the HP-SML device, antigens including CRP, interleukin 6 (IL-6), tumor necrosis factor-alpha (TNF-α), matrix metalloproteinase-9 (MMP-9), and MMP-2 were used. Agarose gels containing 10^5 ng mL^{-1} of each antigen were prepared. The HP-SML device was applied to the agarose gel for 4 seconds. Following this, 99.9 μL of running buffer was added to the filter paper (n = 10). The detection results were analyzed by converting the test line of the strip into grayscale after 10 minutes and assessing the color intensity using ImageJ software.

2.10. *In vivo* test

All animal procedures were performed in accordance with the Guidelines for Care and Use of Laboratory Animals of Dankook University and approved by the Animal Ethics Committee of Dankook University (Approval No. DKU-24-003). Before extracting ISF, the hair on the dorsal skin of 6 week-old SD rats was removed using a depilatory cream. The *in vivo* experiment was designed to evaluate the efficacy of the HP-SML device in distinguishing CRP concentrations in the ISF of normal *versus* inflammatory rats. The inflammatory model was established according to previous studies.[43,44] For this purpose, 100 μL of 1% (w/v) carrageenan solution was injected subcutaneously to induce inflammation over a 4 hour period. After the induction, the HP-SML device was securely attached to the dorsal skin of both normal and inflammatory model rats. The MN was inserted at a 34° angle, and 0.1 μL of ISF was collected over a 20 second period. Subsequently, 99.9 μL of running buffer was added to the collected ISF, and the results were analyzed after 10 minutes (n = 3). Additionally, 1 mL of blood was drawn from the jugular vein to compare serum CRP levels with ISF CRP levels in the same rat. The blood was immediately transferred to a vacutainer (BD Microtainer SST tube) and centrifuged at 13 500 rpm for 10 minutes to obtain serum. The serum was then analyzed using LFA (n = 3).

2.11. Statistical analysis

All experiments were conducted with at least three biological replicates, and results are presented as the mean ± standard deviation. Statistical significance between groups was assessed using an unpaired t-test. In all data, a p-value < 0.05 was considered statistically significant.

3. Results and discussion

3.1. Fabrication of the HP-SML device

The HP-SML device was equipped with a 1 × 5 array of stainless-steel MNs with a length of 1400 μm and a base diameter of 200 μm (Fig. 2A). The filter paper was attached to absorb ISF extracted by the MNs (Fig. 2B), which was fixed under the sample pad of the LFAs (Fig. 2C). The LFAs, connected to the MNs, were mounted onto the strip holder of the Inside part (Fig. 2D(i)). Then, the Outside part was assembled into the Inside part through the rail structure on the side (Fig. 2D(ii) and (iii)).

3.2. Penetration stability test of the HP-SML device

A 3D printer was used to manufacture the inner and outer components of the HP-SML device to replicate the 34° skin penetration angle of MNs. To compare the vertical penetration depth with that of 1400 μm MNs, 750 μm-long MNs were fabricated (see Fig. S2†) and applied to PDMS using the HP-SML device (n = 3) (Fig. 3A). The average insertion angle of the 750 μm MNs through the HP-SML device was approximately 34 ± 0.5°, and the average vertical penetration depth was approximately 350.4 ± 36.5 μm (Fig. 3B). The average insertion angle of the 1400 μm MNs was also 34 ± 0.5°, and the average vertical penetration depth was measured to be 749.2 ± 26.6 μm (Fig. 3C). Furthermore, the reproducibility of the skin penetration angle of MNs inserted through the HP-SML device was confirmed to be excellent. The vertical penetration depth of the 750 μm MN predicted by formula (1) was 396.8 μm, but it was measured at 350.4 μm, showing a difference of 46.4 μm. In contrast, the vertical penetration depth of the 1400 μm MN was 749.2 μm, closely matching the expected 750 μm.

When each MN was applied to pig skin *ex vivo*, a 1 × 5 MN array pattern was clearly observed on the skin surface for both the 750 μm and 1400 μm MNs (Fig. 3D and E). However, for the 750 μm MN, the penetration trace was wider (Fig. 3D),

A

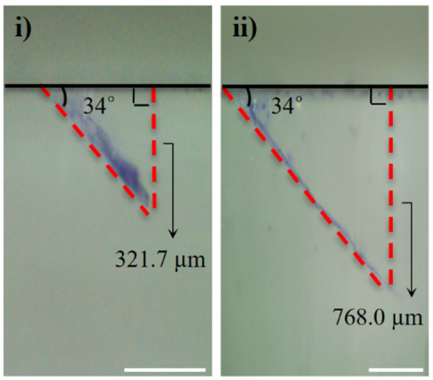

B

750 μm	n=1	n=2	n=3	Avg ±std
Angle(°)	34	33	34	34±0.5
Depth(μm)	321.7	327.5	401.9	350.4±36.5

C

1400 μm	n=1	n=2	n=3	Avg ±std
Angle(°)	34	34	35	34±0.5
Depth(μm)	768.0	711.5	768.0	749.2±26.6

D

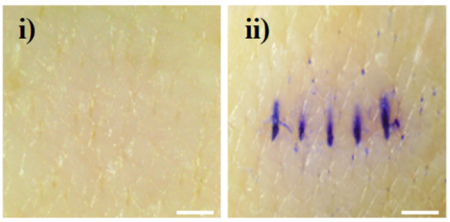

E

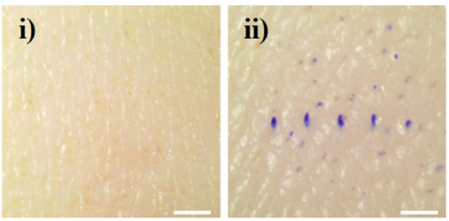

F

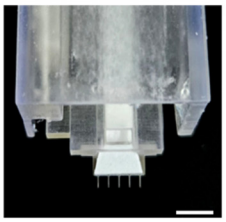

Fig. 3 Skin penetration assessment using the HP-SML device. (A) Optical cross-sectional images of the PDMS after application of the HP-SML device with 750 μm (i) and 1400 μm (ii) length MNs (scale bars = 200 μm). (B) Skin penetration angle and depth using the HP-SML device with 750 μm long MNs. (C) Skin penetration angle and depth using the HP-SML device with 1400 μm long MNs. (D) Optical images of porcine skin *ex vivo* before (i) and after (ii) penetration by the HP-SML device with 750 μm MNs (scale bars = 5 mm). (E) Optical images of porcine skin *ex vivo* before (i) and after (ii) penetration by the HP-SML device with 1400 μm MNs (scale bars = 5 mm). (F) Optical image of the MNs after penetration into porcine skin *ex vivo* (scale bar = 500 μm).

and the trace of the MN that penetrated the PDMS was also stained more thickly (Fig. 3A(i)). This indicates that the penetration force of the 750 μm MN was weaker, leading to the MN being pushed, which reduced penetration accuracy. In contrast, the 1400 μm MN penetrated the skin and PDMS cross-section cleanly (Fig. 3A(ii) and E). After examining the MN status post-application of the HP-SML device to the skin, it was confirmed that none of the MNs were deformed (Fig. 3F). As a result, reproducible skin penetration was achieved through the HP-SML device, and the longer the MN, the more stable and accurate the skin penetration.

3.3. Measurement of ISF extraction capability according to the MN length of the HP-SML device

To investigate the ISF extraction characteristics of the HP-SML device based on the MN length, ISF extraction was compared using MNs with lengths of 750 μm and 1400 μm. First, the relationship between the volume of solution absorbed by the filter paper in the HP-SML device and the wetted area of the filter paper was examined. This relationship was determined by applying up to 5 μL of SRB solution to the filter paper in 0.5 μL increments using a micropipette (Fig. 4A(i)). The results showed that 96.8% of the filter paper was wetted when 5 μL of the solution was applied (Fig. 4A(ii)). The relationship between the volume (x) of the SRB solution applied to the filter paper and the wetted area (y) was graphically represented, yielding the equation $y = 64.2x/(1 + 0.45x)$ (Fig. 4A(iii)). Based on this, ISF extraction from the HP-SML device loaded with 750 μm and 1400 μm MNs was compared. The HP-SML device was applied to 1% (w/v) agarose gel containing SRB solution, and the wetted area of the filter paper was measured every 10 seconds (Fig. 4B). For the 750 μm MN, it was observed that the filter paper was wetted by 96.8 ± 1.62% after 80 seconds of application (Fig. 4B(ii) and S3A(i)†). Over time, the area of the wetted filter paper can be converted into the volume of absorbed solution using the relationship established in Fig. S3A(i)† (see Fig. S3B(i)†). Thus, the relationship between the expected ISF extraction volume and the application time of the HP-SML device with a 750 μm MN was derived (Fig. 4C(i)).

For the 1400 μm MN, when the device was applied for 60 seconds, 97.1 ± 1.9% of the filter paper was wetted (Fig. 4B(iii) and S3A(ii)†). The relationship between the device application time and the area of the soaked filter paper was confirmed (see Fig. S3A(ii)†), which was then converted into the corresponding volume of solution absorbed by the filter paper (see Fig. S3B(ii)†). These data derived the relationship between the expected ISF extraction volume and the application time of the HP-SML device with the 1400 μm MN (Fig. 4C(ii)). Based on the results, it was confirmed that approximately 4.6 μL of solution could be absorbed when the HP-SML device with a 750 μm MN was applied for 80 seconds (Fig. 4C(i)). In contrast, it was predicted that the absorbed solution volume would be about 4.64 μL when the HP-SML device with a 1400 μm MN was applied for 60 seconds (Fig. 4C(ii)). When both devices were used for the same duration, it was confirmed that the 1400 μm

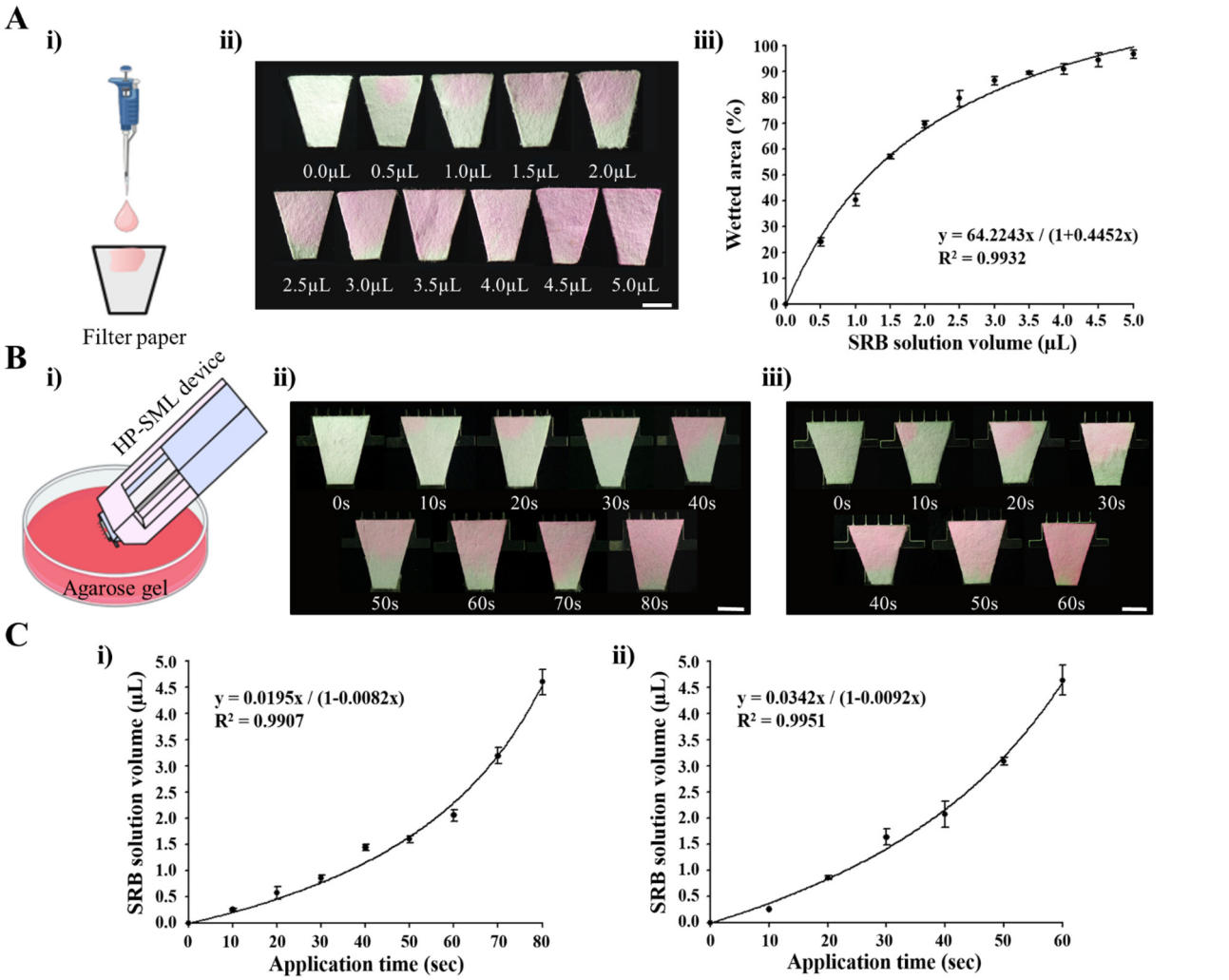

Fig. 4 Quantification of ISF absorbed by filter paper attached to the HP-SML device. (A) Schematic illustration (i) of the addition of SRB solution (0 to 5 μL with 0.5 μL intervals) to the filter paper using a micropipette and an optical image of the wetted filter papers with SRB solutions (ii) (scale bar = 3 mm). Graph and trend formula describing the relationship between the wetted area of the filter paper on the MN and the volume of the SRB solution (iii). (B) Schematic diagram (i) of the application of the HP-SML device to papers with SRB solutions (ii) (scale bar = 3 mm). Graph and trend formula describing the relationship between the wetted area of agarose gel containing SRB for different times (0–80 s at 10 s intervals) and optical images of filter papers when the HP-SML device with a 750 μm MN (ii) and 1400 μm MN (iii) was used (scale bars = 3 mm). (C) Graph and trend line showing the relationship between the application time of the HP-SML device and the volume of SRB solution extracted by the HP-SML device with a 750 μm MN (i) and 1400 μm MN (ii). All the schematics were created using BioRender.

MN extracted a greater volume of ISF than the 750 μm MN. This result demonstrates that the ISF extraction rate increases with the length of the MN.

3.4. CRP detection sensitivity test of the HP-SML device

To confirm the CRP detection sensitivity of the HP-SML device, a detection limit test was performed at CRP concentrations of 0, 10, 10^2, 10^3, 10^4 and 10^5 ng mL^{-1}. According to a previous study, a CRP concentration of 10^4 ng mL^{-1} is considered the threshold for determining the prognostic value following HL treatment.[26] Therefore, the sample volume applied to individual LFAs was optimized to detect CRP at concentrations of 10^4 ng mL^{-1} or higher (see Fig. S4†). First, to determine the detection limit of "single LFAs", 1 μL of CRP antigen at concentrations ranging from 0 to 10^5 ng mL^{-1}, along with 99 μL of running buffer, was loaded onto the sample pad of each LFA. As a result, CRP was detected at concentrations as low as 10^3 ng mL^{-1} (see Fig. S4A and B†). However, to apply LFAs for the prognostic management of HL, the detection limit must be 10^4 ng mL^{-1}. Therefore, an additional detection limit experiment was conducted by reducing the sample volume. The CRP antigen, initially at a concentration of 10^3 ng mL^{-1}, was adjusted to volumes of 0.1, 0.5, and 1 μL, and the results were confirmed (the volume of the running buffer was adjusted so that the total volume, including CRP, was 100 μL) (see Fig. S4C and D†). When the CRP volume was 0.1 μL, CRP was not detected at 10^3 ng mL^{-1}. Therefore, in this study, the CRP volume was set at 0.1 μL and the running buffer at 99.9 μL, and the detection limit experiment was conducted accordingly.

First, the detection limit of "single LFAs" was measured, and it was determined to be 10^4 ng mL^{-1} for CRP (Fig. 5A). This detection limit was assessed using "passive sample loading onto the HP-SML device" (Fig. 5B). A 0.1 μL aliquot of CRP was applied to the HP-SML device using a micropipette, followed by the immediate addition of 99.9 μL of running buffer. The result was evaluated after 10 minutes, confirming a detection limit of 10^4 ng mL^{-1}, indicating that the HP-SML device did not affect the sensitivity of the "single LFAs." Based on these results, the detection limit of the HP-SML device was further assessed (Fig. 5C). A 0.1 μL sample of the solution was extracted from the agarose gel containing CRP by applying the HP-SML device for 4 seconds, and 99.9 μL of running buffer was then immediately added to the filter paper. The detection limit, measured 10 minutes later, was again confirmed to be 10^4 ng mL^{-1}. Therefore, it was demonstrated that the HP-SML device can be effectively applied to the post-treatment prognosis management of HL patients through CRP detection.

3.5. CRP detection specificity test of the HP-SML device

To confirm the specificity of the HP-SML device, experiments were conducted using other inflammatory antigens, including IL-6, MMP-9, TNF-α, and MMP-2, in addition to CRP (Fig. 6). These experiments utilized high concentrations of antigens (10^5 ng mL^{-1}). The results showed that a distinct test line appeared only for CRP, with no detection observed for the other antigens. Thus, the HP-SML device exhibited selectivity for CRP without cross-reactivity with other antigens.

3.6. *In vivo* test

To verify the applicability of the HP-SML device for the prognostic management of HL patients, a CRP detection test was performed using an *in vivo* rat model (Fig. 7). The experiment involved dividing the rats into normal and inflammation model groups. The inflammation model was designed to achieve a blood CRP concentration of 10^4 ng mL^{-1} or higher.[43,44] Based on the results of *in vitro* experiments, 0.1 μL of ISF was extracted from SD rats over 20 seconds using the HP-SML device (Fig. 7A). The *in vivo*

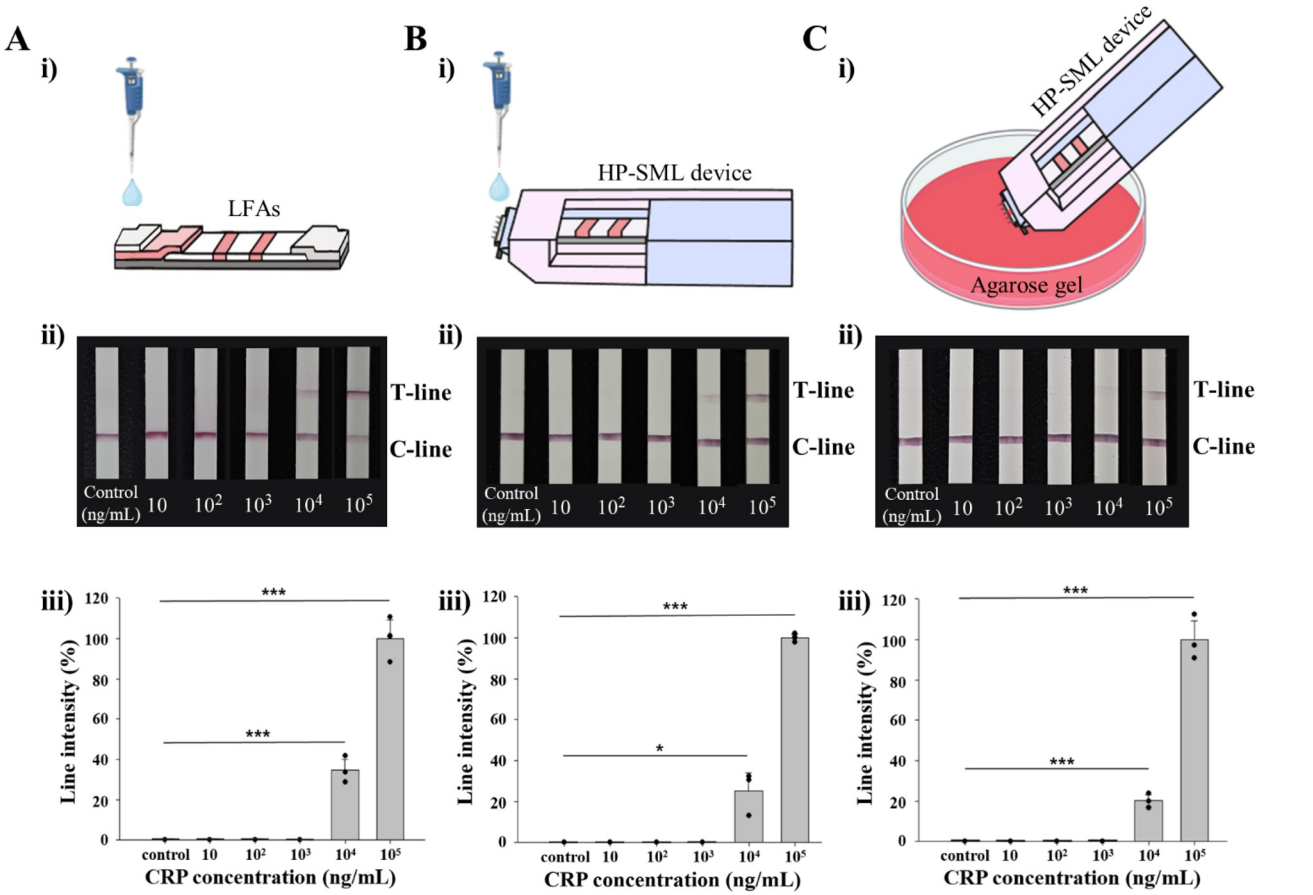

Fig. 5 Limit of detection study of the HP-SML device. (A) The detection limit of "single LFAs" according to the concentration of the CRP solution (0 to 10^5 ng mL^{-1}); a schematic illustration (i), an optical image (ii), and the intensity of the test line analyzed using ImageJ software (iii). (B) The detection limit of "passive sample loading to the HP-SML device" according to the concentration of the CRP solution (0 to 10^5 ng mL^{-1}); a schematic illustration (i), an optical image (ii), and the intensity of the test line analyzed using ImageJ software (iii). (C) The detection limit of "the HP-SML device" from the agarose gel with CRP concentrations ranging from 0 to 10^5 ng mL^{-1}; a schematic illustration (i), an optical image (ii), and the intensity of the test line analyzed using ImageJ software (iii). *, *** indicate significant differences (unpaired *t*-test, $p < 0.05$, 0.001, respectively). All the schematics were created using BioRender.

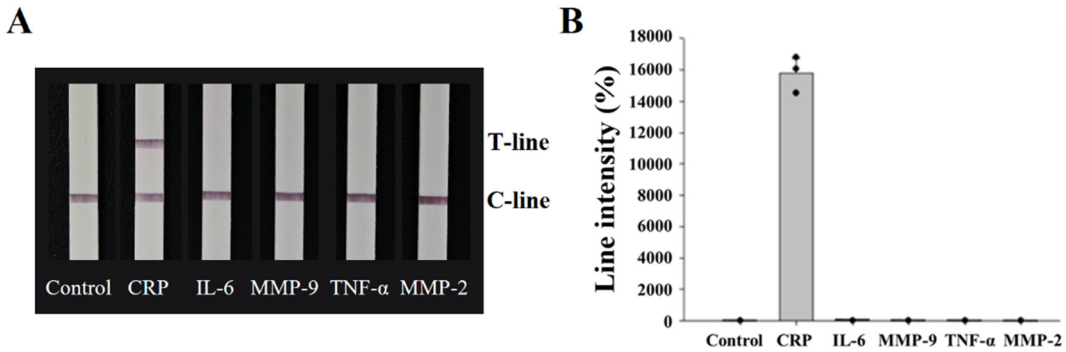

Fig. 6 Specificity assessment using the HP-SML device. (A) Optical micrographs of LFAs illustrating the selective detection of CRP at 10^5 ng mL^{-1} concentration of antigens using the HP-SML device. (B) Quantitative analysis of the test line intensity in (A), performed using ImageJ software. Data are presented as mean ± standard deviation, with a minimum of three independent replicates.

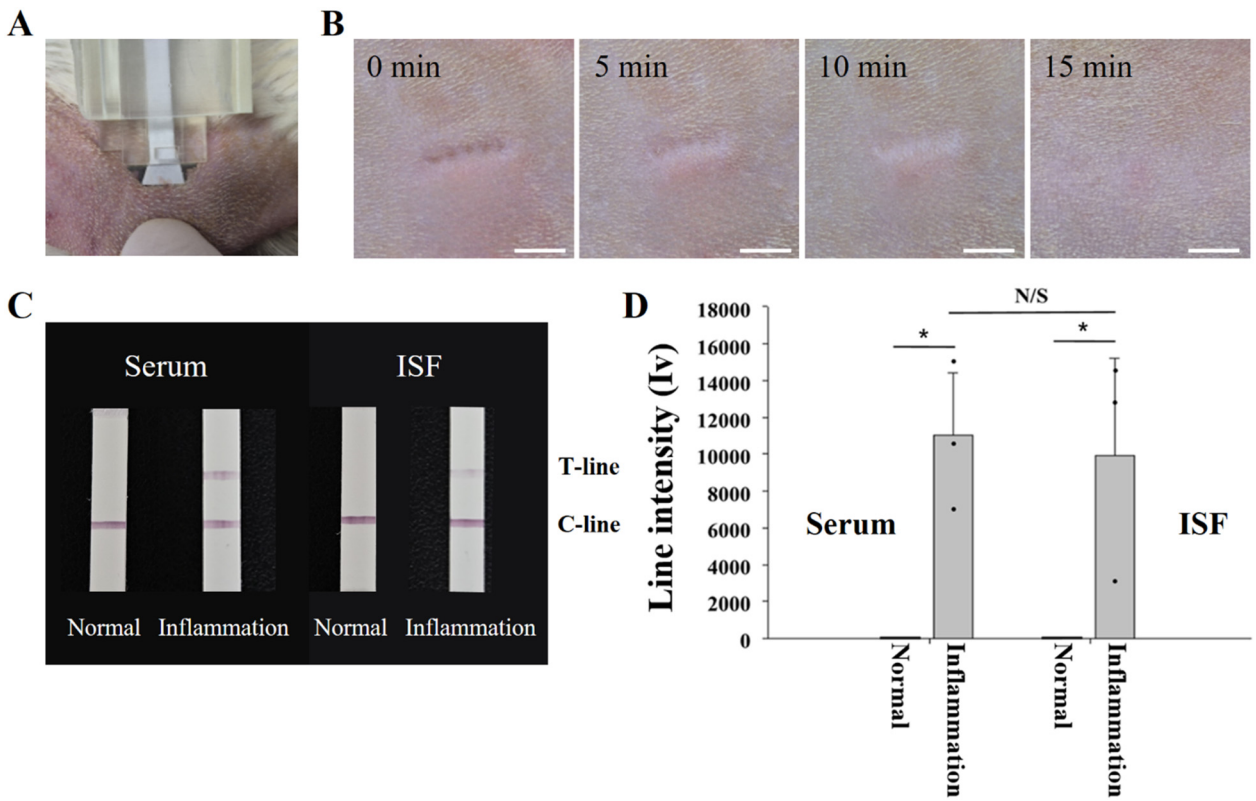

Fig. 7 *In vivo* ISF extraction and diagnostic assessment using the HP-SML device. (A) Optical imaging of *in vivo* ISF extraction employing the HP-SML device. (B) Sequential clinical evaluation of the HP-SML device, captured immediately after device application and at 5, 10, and 15 minutes post-application. (C) Optical images of LFAs detecting CRP in serum and ISF samples from both the normal and inflammation-induced groups. (D) *In vivo* diagnostic outcomes represented by the intensity of the test line in (C), with quantification performed using ImageJ software. * denotes statistically significant differences (unpaired *t*-test, $p < 0.05$).

ISF extraction took longer than under *in vitro* conditions because the ISF content ratio in the skin was lower *in vivo*.[45]

In this study, to independently confirm the *in vivo* ISF extraction rate of the HP-SML device, ISF was extracted from SD rats for 35 seconds (see Fig. S5†). The results indicated that approximately 0.86 μL of ISF was absorbed by the filter paper. The *in vivo* ISF extraction rate of the HP-SML device was 1.5 μL min^{-1}, which is approximately 5 times higher than the extraction rate of 0.3 μL min^{-1} achieved with the existing stainless-steel MN patch.[9]

After extracting the HP-SML device, the stability of rat skin was evaluated at 5 minute intervals (Fig. 7B). MN traces were clearly identifiable immediately after ISF extraction (0 min). By 10 minutes post-extraction, the MN penetration traces had disappeared. Complete recovery of the skin was observed at the 15 minute mark.

Table 1 The performance comparison between the SML device and the HP-SML device

Device	MN length	MN insertion depth	ISF extraction rate (*in vitro*)	ISF extraction rate (*in vivo*)	Note	Ref.
SML device	700 μm	231.5 ± 10.0 μm	3.1 μL min^{-1}	0.3 μL min^{-1}	Device separation required	Yang *et al.*, 2024 (ref. 9)
HP-SML device	1400 μm	749.2 ± 26.6 μm	4.64 μL min^{-1}	1.5 μL min^{-1}	Device separation not required	

Using the HP-SML device, 0.1 μL of ISF was extracted from normal and inflammatory model rats over 20 seconds. Subsequently, 99.9 μL of running buffer was added, and the results were confirmed after 10 minutes. Additionally, serum was collected from the same rats and applied to LFAs to compare the results with ISF (Fig. 7C). CRP was not detected in either serum or ISF in the normal group, while CRP was only in the inflammatory model group. Analysis of the test lines of LFAs using ImageJ software revealed a statistically significant difference in line intensities between the normal and inflammatory model groups for both serum and ISF (Fig. 7D).

Furthermore, there was no statistically significant difference in CRP concentrations between serum and ISF in the inflammatory model. This demonstrates that ISF can substitute blood and that reproducible CRP detection is achievable with a small volume of 0.1 μL. Moreover, *in vivo* tests confirmed that ISF extraction and diagnosis can be completed within 10 minutes and 20 seconds. Therefore, the rapid *in vivo* CRP detection method using the HP-SML device enables continuous on-site management and monitoring of treatment response and the risk of future relapse in HL patients who have completed 6 cycles of chemotherapy.

In this study, we developed the HP-SML device to overcome the limitations of the previously developed SML device.[9] By doubling the MN length, we significantly enhanced the ISF extraction rate. Additionally, we designed the LFA detection area to be externally exposed, allowing for real-time result visualization without requiring device disassembly, thus improving user-friendliness (Table 1). The increased MN length resulted in a larger tissue contact surface area, while the greater penetration depth enabled access to the upper dermal layer, which contains a higher ISF concentration, thereby accelerating ISF extraction.[46] These design improvements were particularly evident in *in vivo* test, where the HP-SML device achieved an ISF extraction rate approximately five times faster than that of the conventional SML device (Table 1). This superior ISF extraction efficiency presents a significant advantage for POC diagnostics and continuous patient monitoring. Given its high-speed ISF extraction capability and enhanced user convenience, the HP-SML device is expected to exhibit greater clinical feasibility and applicability in future medical settings.

4. Conclusions

In this study, we developed the HP-SML device, an advanced MN-based platform designed to significantly enhance ISF extraction speed and facilitate CRP detection. By doubling the MN length and optimizing the MN penetration mechanism, we achieved a 5-fold increase in ISF extraction rate compared to the conventional SML device. The externally exposed LFA detection area further improved usability by allowing direct result visualization without device disassembly, making it ideal for POC applications. *In vivo* studies confirmed that the HP-SML device enables rapid ISF collection (1.5 μL min^{-1}) while maintaining consistent penetration depth and minimal skin damage, with full skin recovery observed within 15 minutes. Additionally, CRP levels detected in ISF correlated well with serum CRP levels, validating ISF as a viable alternative to blood for HL prognosis monitoring. The device achieved a CRP detection limit of 10^4 ng mL^{-1}, meeting the clinical threshold required for effective post-treatment surveillance in HL patients. Furthermore, the HP-SML device demonstrated high specificity for CRP, showing no cross-reactivity with other inflammatory markers such as IL-6, TNF-α, MMP-9, and MMP-2.

Despite these promising results, certain limitations remain. Variations in skin thickness and physiological properties due to anatomical site, age, sex, or ethnicity may affect device performance, indicating the need for standardized usage protocols in future clinical applications. Moreover, as the current system detects only a single biomarker, expanding the HP-SML device to support multiplex detection will be essential for improving diagnostic reliability and extending its application scope.

Given its enhanced efficiency, user-friendly design, and strong diagnostic accuracy, the HP-SML device represents a promising tool for continuous HL relapse monitoring and broader POC diagnostic applications. Future work will focus on addressing the current limitations and advancing the system toward personalized patient management in oncology and inflammatory disease monitoring.

Data availability

The authors report that the results of this study are available within the manuscript and ESI.†

Author contributions

Soo-bin Yu: validation, data curation, writing – original draft preparation, writing – review and editing, visualization, formal analysis. Jae Hwan Jung: conceptualization, writing – review and editing, investigation, methodology, resources,

supervision, project administration. All authors have read and agreed to the published version of the manuscript.

Conflicts of interest

There are no conflicts to declare.

Acknowledgements

The authors thank Prof. Jun Hee Lee at the Institute of Tissue Regeneration Engineering (ITREN) for his assistance with the animal experiments.

References

1 K. M. Saifullah, A. Mushtaq, P. Azarikhah, P. D. Prewett, G. J. Davies and Z. Faraji Rad, *Microsyst. Nanoeng.*, 2025, **11**, 3.
2 P. P. Samant, M. M. Niedzwiecki, N. Raviele, V. Tran, J. Mena-Lapaix, D. I. Walker, E. I. Felner, D. P. Jones, G. W. Miller and M. R. Prausnitz, *Sci. Transl. Med.*, 2020, **12**, eaaw0285.
3 S. Kim, M. S. Lee, H. S. Yang and J. H. Jung, *Sci. Rep.*, 2021, **11**, 14018.
4 C. Kolluru, R. Gupta, Q. Jiang, M. Williams, H. G. Derami, S. Cao, R. K. Noel, S. Singamaneni and M. R. Prausnitz, *ACS Sens.*, 2019, **4**, 1569–1576.
5 N. Xu, W. Xu, M. Zhang, J. Yu, G. Ling and P. Zhang, *Adv. Mater. Technol.*, 2022, **7**, 2101595.
6 Y. Xie, J. He, W. He, T. Iftikhar, C. Zhang, L. Su and X. Zhang, *Adv. Sci.*, 2024, **11**, 2308716.
7 X. Yuan, O. Ouaskioud, X. Yin, C. Li, P. Ma, Y. Yang, P.-F. Yang, L. Xie and L. Ren, *Micromachines*, 2023, **14**, 1452.
8 X. Zhang, W. Zhang, W. Wu and J. Chen, *Microchem. J.*, 2023, **195**, 109477.
9 G. R. Yang, W. Kim and J. H. Jung, *Biosens. Bioelectron.*, 2024, **263**, 116590.
10 M. A. Weniger and R. Küppers, *Leukemia*, 2021, **35**, 968–981.
11 M. A. Piris, L. J. Medeiros and K.-C. Chang, *Pathology*, 2020, **52**, 154–165.
12 A. Satou, T. Takahara and S. Nakamura, *Cancers*, 2022, **14**, 2647.
13 T. J. Voorhees and A. W. Beaven, *Cancers*, 2020, **12**, 2887.
14 O. Potre, M. Pescaru, A. Sima, I. Ionita, R. Tudor, E. Borsi, M. Samfireag and C. Potre, *Medicina*, 2021, **57**, 1026.
15 G. Bentolila and A. Pavlovsky, *Leuk. Lymphoma*, 2020, **61**, 1548–1554.
16 A. Al-Ibraheem, F. M. Mottaghy and M. E. Juweid, *Semin. Nucl. Med.*, 2023, **53**, 303–319.
17 L. J. Jensen, J. M. Rogasch, D. Kim, J. Rießelmann, C. Furth, H. Amthauer, B. Hamm, I. G. Steffen, T. Elgeti and S. N. Nagel, *Sci. Rep.*, 2022, **12**, 20008.
18 F. Keyvani, H. Zheng, M. R. Kaysir, D. F. Mantaila, P. Ghavami Nejad, F. A. Rahman, J. Quadrilatero, D. Ban and M. Poudineh, *Angew. Chem.*, 2023, **62**, e202301624.
19 J. D. Chalmers, A. Singanayagam and A. T. Hill, *Am. J. Med.*, 2008, **121**, 219–225.
20 A. Onat, G. Can and G. Hergenç, *Metabolism*, 2008, **57**, 207–214.
21 F. Liu, L. Li, M. Xu, J. Wu, D. Luo, Y. Zhu, B. Li, X. Song and X. Zhou, *J. Clin. Virol.*, 2020, **127**, 104370.
22 W. M. Fakanya and I. E. Tothill, *Biosens. Bioelectron.*, 2014, **4**, 340–357.
23 H. Sohrabi, H. K. Kordasht, P. Pashazadeh-Panahi, P. Nezhad-Mokhtari, M. Hashemzaei, M. R. Majidi, J. Mosafer, F. Oroojalian, A. Mokhtarzadeh and M. de la Guardia, *Microchem. J.*, 2020, **158**, 105287.
24 D. Stringer, P. Braude, P. K. Myint, L. Evans, J. T. Collins, A. Verduri, T. J. Quinn, A. Vilches-Moraga, M. J. Stechman and L. Pearce, *Int. J. Epidemiol.*, 2021, **50**, 420–429.
25 M. Fazal, *Korean J. Clin. Lab. Sci.*, 2021, **53**, 201–207.
26 E. Negreiros, T. M. B. Silveira, S. C. Fortier and C. S. Chiattone, *Hematol. Transfus. Cell Ther.*, 2024, **46**, 53–58.
27 A. Wieland, R. Kerbl, A. Berghold, W. Schwinger, G. Mann and C. Urban, *Med. Pediatr. Oncol.*, 2003, **41**, 21–25.
28 Y.-J. Li, Z.-M. Li, Y. Xia, J.-J. Huang, H.-Q. Huang, Z.-J. Xia, T.-Y. Lin, S. Li, X.-Y. Cai and Z.-J. Wu-Xiao, *PLoS One*, 2013, **8**, e64158.
29 J. Zhao, J. Lv, G. Ling and P. Zhang, *Int. J. Biol. Macromol.*, 2024, **254**, 127745.
30 Z. F. Rad, P. D. Prewett and G. J. Davies, *Beilstein J. Nanotechnol.*, 2021, **12**, 1034–1046.
31 A. M. Downs, A. Bolotsky, B. M. Weaver, H. Bennett, N. Wolff, R. Polsky and P. R. Miller, *Biosens. Bioelectron.*, 2023, **236**, 115408.
32 E. M. Cahill, S. Keaveney, V. Stuettgen, P. Eberts, P. Ramos-Luna, N. Zhang, M. Dangol and E. D. O'Cearbhaill, *Acta Biomater.*, 2018, **80**, 401–411.
33 W. Deenin, N. Khongchareonporn, K. Ruxrungtham, C. Ketloy, N. Hirankarn, K. Wangkanont, S. Rengpipat, A. Yakoh and S. Chaiyo, *Anal. Chem.*, 2024, **96**, 5407–5415.
34 S. D. Souza, W. Obeid, J. Hernandez, D. Hu, Y. Wen, D. G. Moledina, A. Albert, A. Gregg, A. Wheeler and H. T. Philbrook, *Sci. Rep.*, 2024, **14**, 8516.
35 Z. Ma, J. Guo, L. Jiang and S. Zhao, *Talanta*, 2024, **267**, 125268.
36 J. M. A. Ershaid, L. K. Vora, F. Volpe-Zanutto, A. H. Sabri, K. Peng, Q. K. Anjani, P. E. McKenna, A. Ripolin, E. Larrañeta and H. O. McCarthy, *Biomater. Adv.*, 2023, **153**, 213526.
37 Y. Wu, L. K. Vora, R. F. Donnelly and T. R. R. Singh, *Drug Delivery Transl. Res.*, 2023, **13**, 2142–2158.
38 M. B. McGuckin, A. R. Hutton, E. R. Davis, A. H. Sabri, A. Ripolin, A. Himawan, Y. A. Naser, R. Ghanma, B. Greer and H. O. McCarthy, *Mol. Pharmaceutics*, 2024, **21**, 2512–2533.
39 K. Ita, *Pharmaceutics*, 2015, **7**, 90–105.
40 B. Shriky, M. Babenko and B. R. Whiteside, *Gels*, 2023, **9**, 806.
41 D. D. Zhu, Y. R. Tan, L. W. Zheng, J. Z. Lao, J. Y. Liu, J. Yu and P. Chen, *ACS Appl. Mater. Interfaces*, 2023, **15**, 14146–14154.
42 K. Choudhary, N. Mathur, O. Choudhary and U. Pillai, *Adv. Biol. Res.*, 2008, **2**, 83–89.

43 J. C. Fehrenbacher, M. R. Vasko and D. B. Duarte, *Curr. Protoc. Pharmacol.*, 2012, **56**, 5.4.1–5.4.4.
44 H. Zhang, C. Shang, Z. Tian, H. K. Amin, R. B. Kassab, A. E. Abdel Moneim and Y. Zhang, *Mediators Inflammation*, 2020, **2020**, 8508906.
45 M. Friedel, I. A. Thompson, G. Kasting, R. Polsky, D. Cunningham, H. T. Soh and J. Heikenfeld, *Nat. Biomed. Eng.*, 2023, **7**, 1541–1555.
46 L. Qiu, S. Wang, Z. Wang, Y. Ma and Y. Feng, *Int. J. Heat Mass Transfer*, 2022, **197**, 123328.